J. metamorphic Geol., 2009, **27**, 153–165 doi:10.1111/j.1525-1314.2009.00812.x

A thermodynamic model for titanium and ferric iron solution in biotite

L. TAJČMANOVÁ,[1,2]* J. A. D. CONNOLLY[3] AND B. CESARE[1]
[1]*Department of Geosciences, University of Padova, via Giotto 1, I-35137 Padova, Italy (lucataj@gmail.com)*
[2]*Czech Geological Survey, Klárov 3, 118 21 Praha 1, Czech Republic*
[3]*Department of Earth Sciences, Swiss Federal Institute of Technology, CH-8092, Zürich, Switzerland*

ABSTRACT Recent crystallographic data indicate that in biotite Ti orders preferentially onto the M2 octahedral site rather than onto the M1 site as assumed in previous solution models for K_2O–FeO–MgO–Al_2O_3–SiO_2–H_2O–TiO_2–O_2 (KFMASHTO) biotite. In view of these data, we reformulate and reparameterize former biotite solution models. Our reparameterization takes into account Fe–Mg order–disorder and ferric iron contents of natural biotite as well as both natural and experimental observations on biotite Ti-content over a wide range of physicochemical conditions. In comparison with previous biotite models, the new model reproduces the Ti-content and stability field of biotite as constrained by experiments with significantly better accuracy. The predictive power of the model is tested by comparison with petrologically well-characterized natural samples of SiO_2-saturated and SiO_2-undersaturated rocks that were not used in the parameterization. In all these tests, the reformulated model performs well.

Key words: biotite thermodynamic model; phase equilibria; thermodynamic properties.

INTRODUCTION

The ubiquitous occurrence of biotite in metamorphic rocks has motivated efforts to develop a thermodynamic model for its crystal chemistry (Powell & Holland, 1999; White *et al*., 2000, 2007; Holland & Powell, 2006). Recent studies have focused on the role of ferric iron and titanium in extending the stability field of K_2O–FeO–MgO–Al_2O_3–SiO_2–H_2O (KFMASH) biotite in *P–T* space (Harley, 1989; Carswell & O'Brien, 1993; Vielzeuf & Montel, 1994; Patiño Douce & Beard, 1995, 1996; White *et al*., 2000, 2002, 2007). Experimental observations (Patiño Douce & Johnston, 1991; Vielzeuf & Clemens, 1992; Patiño Douce *et al*.,1993; Stevens *et al*., 1997) and calculated petrogenetic grids for the K_2O–FeO–MgO–Al_2O_3–SiO_2–H_2O–TiO_2–O_2 (KFMASHTO) and Na_2O–CaO–K_2O–FeO–MgO–Al_2O_3–SiO_2–H_2O–TiO_2–O_2 (NCKFMASHTO) systems (Clarke *et al*., 1989; White *et al*., 2000, 2002, 2007) suggest that in these systems biotite melting may occur at temperatures nearly 50 °C higher than it does in the KFMASH and NCKFMASH systems.

In the most common biotite polytype (*1M*, space group *C2/*m, e.g. Mercier *et al*., 2006) there is one M1 octahedral site and two equivalent M2 octahedral sites that are *trans*- and *cis*-coordinated by hydroxyl groups, respectively. Structural refinements show that for typical natural compositions the M1 site is larger than the two M2 (e.g. Brigatti & Guggenheim, 2002). On the basis of these geometric and additional energetic considerations (Toraya, 1981), the M2 sites are more likely to host cations with high ionic charge and small ionic radius, such as Ti^{4+}, especially if charge balance is maintained by deprotonation of the *cis*-coordinated hydroxyl groups. This preference of Ti for M2 has been confirmed by several structural studies of natural biotite (e.g. Cruciani & Zanazzi, 1994; Cesare *et al*., 2003; Ventruti *et al*., 2009).

The exchange mechanism for Ti solution in KFMASH biotite has been the subject of numerous studies (reviews in Waters & Charnley, 2002; Cesare *et al*., 2003; Scordari *et al*., 2006), suggesting that the dominant exchange mechanism at upper amphibolite and granulite facies metamorphic conditions, as well as in magmatic settings, is a Ti-oxy substitution, i.e. the substitution of Ti for a divalent octahedral cation charge balanced by deprotonation in the hydroxyl site. Currently, the only thermodynamic solution model to account for this exchange in biotite is that of White *et al*. (2007), which assumes that titanium orders onto the M1 site. Although the octahedral site occupancy of Al is controversial (cf., e.g. Cruciani & Zanazzi, 1994; Brigatti *et al*., 2000a; Berman *et al*., 2007), here we follow Powell & Holland (1999) in assuming that

**Present address (from March 2009)*: AB Mineralogy-Petrology, Institute of Geological Sciences, Freie Universität, Malteserstr. 74-100 (Haus N), 12249 Berlin, Germany.

© 2009 Blackwell Publishing Ltd

octahedrally coordinated Al is introduced by a Tschermak-type exchange and partitions preferentially onto the M1 site, as first proposed by Circone & Navrotsky (1992) and supported by the recent study of Ventruti *et al.* (2009). The ferric iron site populations and exchange mechanisms in KFMASH biotite are ambiguous in that early Mössbauer spectroscopic data suggested that Fe^{3+} is tetrahedrally coordinated (Guidotti & Dyar, 1991), whereas more recent data indicate that Fe^{3+} partitions preferentially onto the octahedral sites (Cruciani & Zanazzi, 1994; Virgo & Popp, 2000; Mesto *et al.*, 2006). In the case of octahedral Fe^{3+}, there is crystallographic evidence for both Tschermak-type ($R^{2+} + Si = Fe^{3+} + Al$) and Fe-oxy ($Fe^{2+} + OH^- = Fe^{3+} + O^{2-}$) exchanges (e.g. Laurora *et al.*, 2007). In initial attempts to formulate a KFMASHTO biotite model, we were unable to fit the Ti-content of natural biotite if an Fe-oxy exchange was assumed. Accordingly, it is assumed that Fe^{3+} is introduced by a Tschermak-type exchange and, by analogy with Al^{3+}, that this exchange favours the M1 site (Cesare *et al.*, 2003).

Comparison of biotite compositions predicted with the White *et al.* (2007) solution model and experimental determinations (Vielzeuf & Montel, 1994) for a metagreywacke composition reveal that at granulite facies conditions the predicted Ti-content [in atoms per formula unit (p.f.u.) normalized on the basis of 11 O atoms] of biotite is significantly lower (Ti = 0.21 p.f.u. at the highest temperature limit of the biotite stability field) than that observed experimentally (Ti = 0.28 p.f.u.; Fig. 1a). Additionally, the experimentally determined biotite stability field is larger than that predicted by the thermodynamic model. The magnitude of these discrepancies is significantly larger than the experimental error and motivated us to reparameterize the biotite solution model. In undertaking this reparameterization we build on the KFMASH biotite model of Holland & Powell (2006), exploiting the aforementioned crystallographic data that suggest that Ti is ordered onto the M2 sites rather than onto the M1 site as assumed by White *et al.* (2007). The resulting model was then tested against experimental data (Vielzeuf & Montel, 1994; Montel & Vielzeuf,

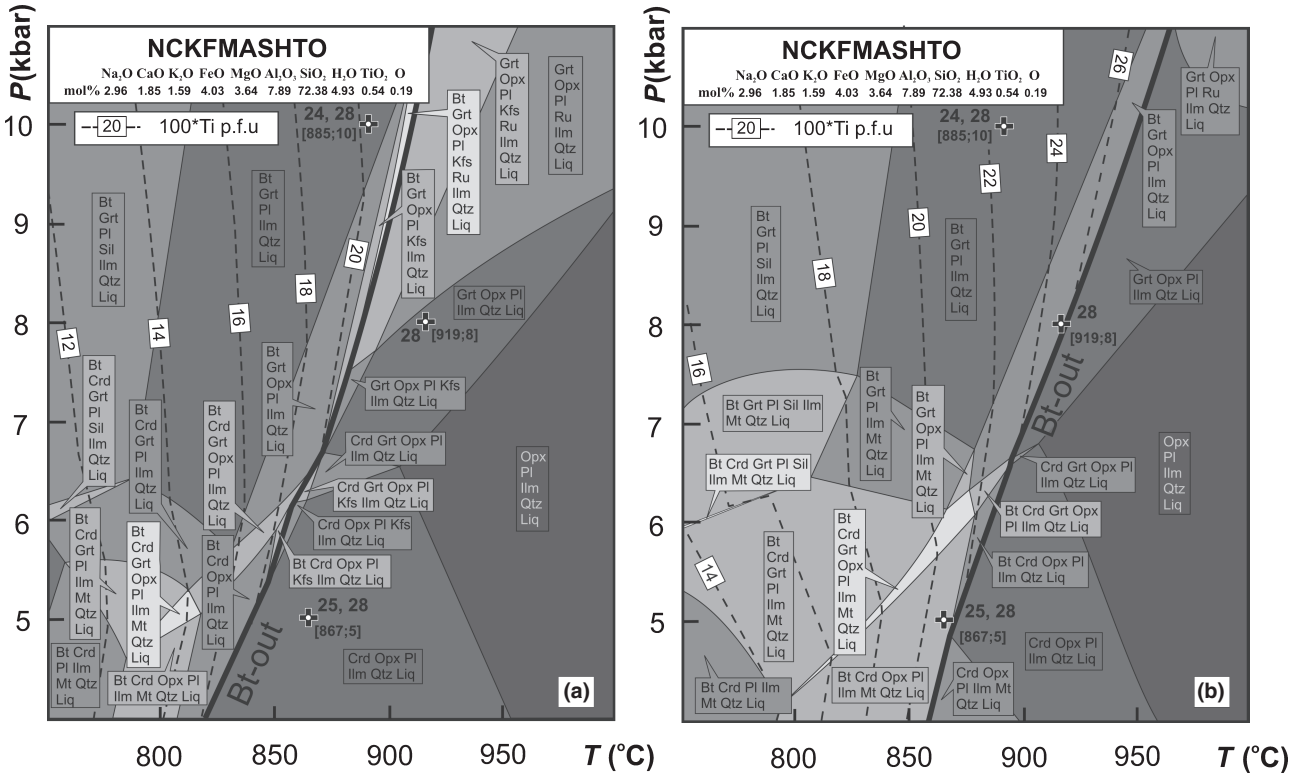

Fig. 1. *P–T* section calculated in Na_2O-CaO-K_2O-FeO-MgO-Al_2O_3-SiO_2-H_2O-TiO_2-O_2 (NCKFMASHTO) system for metagreywacke bulk rock compositions taken from the experimental work of Vielzeuf & Montel (1994). System composition (in mol.%) used for calculation is presented in upper left inset. (a) The *P–T* section was calculated using THERMOCALC 3.26 (Powell *et al.*, 1998; 2007 version) and the data set 5.5 (Holland & Powell, 1998; November 2003 upgrade), in the system NCKFMASHTO with the biotite, garnet and melt models from White *et al.* (2007), ilmenite from White *et al.* (2000), feldspar from Holland & Powell (2003), paragonite–muscovite from Coggon & Holland (2002) and other models from THERMOCALC documentation (Powell & Holland, 2004). (b) *P–T* section calculated using the present biotite model parameterization and Perple_X computer program (Connolly, 2005). Dashed lines are contours for Ti p.f.u. in biotite. The thick black line represents the upper limit of biotite stability field. The points (black crosses) distributed in the diagram correspond to the representative measured data for biotite composition from the experiment (Montel & Vielzeuf, 1997). They are labelled by [*T* (°C); *P* (kbar)] coordinates and Ti-content multiplied by 100 assuming biotite normalized on the basis of 11 O atoms. The coordinates of three representative points are [885; 10]; [919; 8]; [867; 5].

© 2009 Blackwell Publishing Ltd

1997) and selected amphibolite to granulite facies natural samples covering a wide range of metamorphic and anatectic conditions in both silica-saturated and -undersaturated environments.

THE KFMASH BIOTITE MODEL

Powell & Holland (1999) and Holland & Powell (2006) formulated a non-ideal order–disorder model for KFMASH biotite between the end-members phlogopite, annite, eastonite and ordered biotite (obi)

$$\tfrac{2}{3}\ \text{phlogopite} + \tfrac{1}{3}\ \text{annite} = \text{obi}, \qquad (1)$$

with site occupancies as summarized in Table 1. Without modification, the parameterization of Holland & Powell (2006) predicts excessive Al-content in biotite (Fig. 2a). This result is not surprising in that the enthalpy of the ordering reaction $\Delta H^0_{\text{order}} = -2$ kJ mol^{-1} (Holland & Powell, 2006) was derived assuming a value for the ordering parameter

$$Q \equiv z^{\text{M2}}_{\text{Mg}} - z^{\text{M1}}_{\text{Mg}}$$

of 0.1, where z^{j}_{Mg} is the atomic fraction of Mg in site j. Thus, the assumed value of the intracrystalline partition coefficient $K_{\text{d}}^{\text{M1/M2}} = (\text{Fe/Mg})_{\text{M1}}/(\text{Fe/Mg})_{\text{M2}}$ is likewise low. Crystal chemical data (Brigatti *et al.*, 2000b) indicate that low intercrystalline partition coefficients are typical of biotite in which the site fraction of Al on the octahedral site is high, and therefore atypical for biotite in common metamorphic rocks (Fig. 2a). In view of these considerations, the $\Delta H^0_{\text{order}}$ is constrained here from the most ordered natural biotite reported by Brigatti *et al.* (2000b) ($Q = 0.30$ at 973 K). Assuming that all other parameters of the Holland & Powell (2006) model are correct, and following their derivation, the enthalpy of the ordering reaction is then $\Delta H^0_{\text{order}} = -6.8$ kJ mol^{-1}. The increase in $\Delta H^0_{\text{order}}$ lowers the octahedral Al-content predicted for KFMASH biotite, an effect that improves the match with natural observations (Fig. 2b).

THE KMASHTO BIOTITE MODEL

Following the strategy of White *et al.* (2000, 2007) the KFMASH biotite model was extended for the KFMASHTO system by introducing titanium biotite (tbi) and ferric biotite (fbi) end-members (Table 1; see Appendix for the complete formulation of the model and its parameterization). The vibrational and volumetric components of tbi and fbi equations of state were estimated as stoichiometrically weighted linear combinations of the properties of phases with known thermodynamic properties; specifically,

$$\text{phlogopite} - \text{brucite} + \text{rutile} = \text{tbi} \qquad (2)$$

and

$$\text{eastonite} - \tfrac{1}{2}\ \text{corundum} + \tfrac{1}{2}\ \text{hematite} = \text{fbi} \qquad (3)$$

with the properties of phlogopite, brucite, rutile, eastonite, corundum and hematite taken from Holland & Powell (1998, as revised in 2003). The third law of entropy estimated by reaction (2) was increased by $2R\ln(2)$ to account for the disorder of Ti and Mg on the M2 site of the tbi end-member. The Gibbs energies of formation from the elements of tbi and fbi were estimated by regression of natural and experimental phase equilibria as detailed below. The biotite in the samples selected for these analyses has dilute Ti- and Fe^{3+}-contents. This criterion was introduced to ensure proximity to Henry's law limiting behaviour for the dilute end-members. In the Henry's law limit (e.g. Lasaga & Burnham, 1979), if the interaction energies involving the dilute end-member are of comparable magnitude then the partial molar Gibbs energy of the end-member differs from that of the pure end-member by an amount that is a function of the non-dilute end-members and a constant that approximates the interaction energies of the dilute end-member. This latter condition was assumed here, in which case Henryian solution behaviour gives rise to pseudo-ideal solution behaviour in which the interaction parameters involving the dilute end-member are zero, provided a Henry's law reference state is adopted for the dilute end-member. Thus, the Gibbs energies of formation for tbi and fbi obtained below are for the Henry's law reference state, i.e. that of the pure end-member at infinite dilution and the pressure and temperature of interest. In the Henryian limit, interactions between dilute end-members are negligible; thus the influence of minor impurities, notably Mn solution, were discounted.

Table 1. End-members and site distribution for KFMASHTO biotite.

End-member		Formula	Site distribution			
			M1	M2	T1	H
	fbi	$K(Mg_2Fe^{3+})(Al_2Si_2)O_{10}(OH)_2$	Fe^{3+}	Mg_2	Al_2	$(OH)_2$
	tbi	$K(Mg_2Ti)(AlSi_3)O_{10}(O)_2$	Mg	TiMg	AlSi	O_2
	east	$K(Mg_2Al)(Al_2Si_2)O_{10}(OH)_2$	Al	Mg_2	Al_2	$(OH)_2$
	ann	$KFe_3(AlSi_3)O_{10}(OH)_2$	Fe	Fe_2	AlSi	$(OH)_2$
	phl	$KMg_3(AlSi_3)O_{10}(OH)_2$	Mg	Mg_2	AlSi	$(OH)_2$
Ordered:	obi	$K(Mg_2Fe)(AlSi_3)O_{10}(OH)_2$	Fe	Mg_2	AlSi	$(OH)_2$

Ferric-biotite end-member (fbi)

White *et al.* (2000, 2007) also defined the ferric biotite end-member from reaction (3); however, its Gibbs energy had to be recalibrated to account for the enthalpy of the ordering reaction for biotite adopted here. Natural observations (Williams & Grambling, 1990) for the equilibrium

$$3\ \text{fbi} + \tfrac{1}{2}\ \text{almandine} + 1\ \text{sillimanite/kyanite} = 3\ \text{eastonite} + 2.5\ \text{quartz} + 1.5\ \text{magnetite}. \qquad (4)$$

© 2009 Blackwell Publishing Ltd

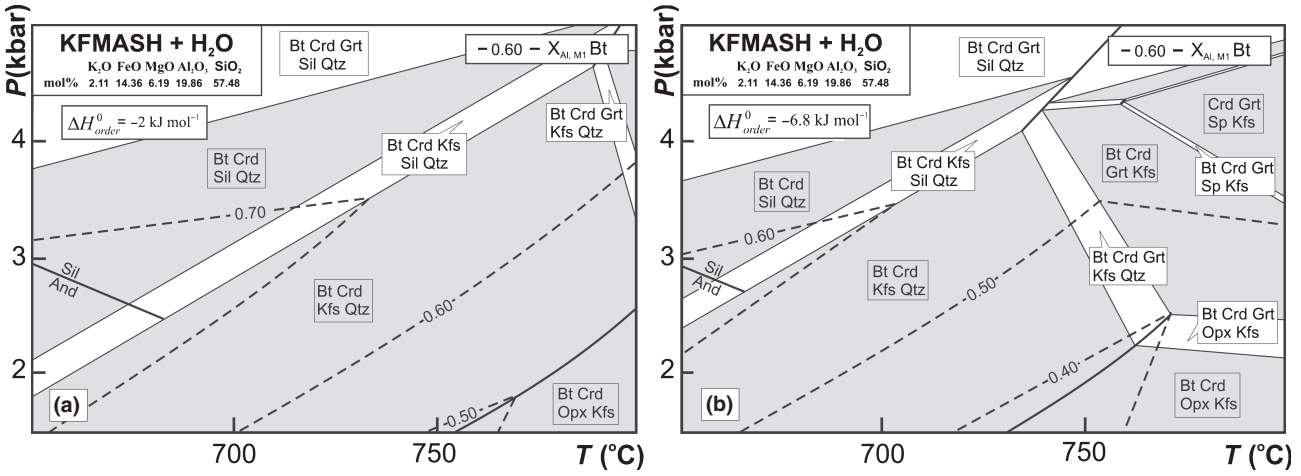

Fig. 2. *P–T* section calculated in K_2O-FeO-MgO-Al_2O_3-SiO_2-H_2O (KFMASH) system with H_2O in excess for metapelitic bulk rock compositions taken from fig. 5c of Pitra & de Waal (2001). System composition (in mol.%) used for calculation is presented in upper left inset. Broken lines are contours for $X_{Al,\ M1}$ in biotite. (a) For the enthalpy of the ordering reaction $\Delta H^0_{order} = -2$ kJ mol^{-1} (Holland & Powell, 2006); (b) for the enthalpy of the ordering reaction $\Delta H^0_{order} = -6.8$ kJ mol^{-1} (this work). According to the published biotite compositional data, the $X_{Al,M1}$ in biotite should range from 0.32 to 0.51 in the (Grt)-Bt-Crd-Kfs-Qtz fields. The *P–T* range of the diagram was reduced compared with fig. 5c in Pitra & de Waal (2001).

Table 2. Biotite source data and regression analysis for δH_{tbi} and δH_{fbi}.

Ti (p.f.u)	*T* (K)	*P* (bar)	δH_{tbi} (J mol^{-1})	Fe^{3+} (p.f.u)	*T* (K)	*P* (bar)	δH_{fbi} (J mol^{-1})
0.07	823	4500	92 551.04	0.14	823	4500	8306.64
0.08	773	4000	87 825.17	0.16	823	4500	6942.51
0.09	773	4000	86 004.85	0.27	823	4500	1511.85
0.10	773	4000	86 926.94	0.21	823	4500	3467.12
0.11	823	4500	87 275.44	0.17	823	4500	6427.02
0.12	823	4500	85 211.08	0.17	823	4500	6502.14
0.13	823	4500	82 354.66	0.15	823	4500	8275.39
0.19	1098	10 000	101 433.1	0.20	773	4000	4931.81
0.20	1082	5000	97 977.97	0.20	873	5000	4736.55
0.21	1098	7000	93 797.8	0.17	873	5000	7032.21
0.22	1148	8000	96 789.39	0.21	873	5000	3538.13
0.23	1123	7000	90 521.66	0.19	873	5000	4802.44
0.24	1198	7000	90 236.11	0.19	873	5000	5100.46
0.26	1148	7000	86 315.63	0.18	873	5000	6307.57
0.27	1173	7000	86 381.44				**5562.99**
0.28	1158	10 000	83 829.14				
0.29	1137	8000	81 082.02				
0.29	1198	10 000	88 869.22				
0.30	1248	10 000	89 347.36				
0.33	1223	10 000	83 906.79				
0.34	1223	13 000	86 908.82				
0.34	1173	8000	61 902.23				
0.35	1173	8000	60 397.61				
0.35	1198	15 000	78 535.37				
0.36	1223	7000	74 044.14				
0.39	1203	12 500	73 094.61				
0.39	1223	15 000	77 535.97				
0.43	1233	12 500	67 915				
			84 248.95				

ANOVA

	tbi						fbi					
	Coefficients	Standard Error	*t* Stat	*P*-value	Lower 95%	Upper 95%	Coefficients	Standard Error	*t* Stat	*P*-value	Lower 95%	Upper 95%
ANOVA for the regression model $\delta G = \delta H - T\delta S + P\delta V$												
δH (J mol^{-1})	95 285.93	13 911.21	6.85	0.00	66 635.25	123 936.61	−3.392e+19	2.1222e+19	−1.5983344	0.138274241	−8.063e+19	1.279e+19
δS (J K^{-1} mol^{-1})	4.73	17.05	−0.28	0.78	−39.84	30.38	−9.0938e+16	5.68953e+16	1.59833441	0.138274241	−3.429e+16	2.162e+17
δV (J bar^{-1} mol^{-1})	−0.73	0.88	−0.83	0.41	−2.54	1.08	−9.094e+15	5.68953e+15	−1.5983344	0.138274241	−2.162e+16	3.429e+15
ANOVA for the regression model $\delta G = \delta H$; (i.e., $\delta S = \delta V = 0$)												
δH (J mol^{-1})	84 248.95	1864.43	45.1874	5.57e−27	80 423.446	88 074.453	5562.99	513.06	10.8428005	6.98194e−08	4454.5934	6671.3834

© 2009 Blackwell Publishing Ltd

were used for the recalibration. This equilibrium was not considered by White *et al.* (2000, 2007), but is employed here to avoid the use of samples in which ferric iron contents are known only by indirect estimates. In all samples considered, the ferric iron content of biotite was measured directly by Mössbauer spectroscopy or by wet chemistry. The data used for calibration are from phase assemblages thought to have equilibrated at temperatures and pressures of 500–600 °C and 4–5 kbar, respectively, with ferric iron contents in biotite ranging from 0.14 to 0.27 Fe^{3+} p.f.u. Magnetite, quartz and sillimanite were assumed to be pure and the almandine–pyrope–grossular solution model of White *et al.* (2007) was used for garnet. Regression analysis (Table 2) yields a Henry's law reference state Gibbs energy of formation (Eq. A.3, Appendix) from the elements for ferric biotite of -5526.53 ± 0.5 kJ mol^{-1} at 298 K and 0.1 MPa. The residuals for the regression model show no significant P–T dependence, indicating that the vibrational and volumetric components of the fbi equation of state, as estimated from reaction (3), are adequate to represent the data.

Titanium-biotite end-member (tbi)

The calibration of the titanium-biotite end-member was completed using natural (Williams & Grambling, 1990) and experimental (Vielzeuf & Montel, 1994; Patiño Douce & Beard, 1995) observations of the equilibrium

$$3 \text{ phlogopite} + 3 \text{ eastonite} + 6 \text{ ilmenite} = 12 \text{ quartz} + \text{pyrope} + 2 \text{ almandine} + 6 \text{ tbi} + 6 \text{ } H_2O. \quad (5)$$

The data span a wide range of P–T conditions (500–960 °C and 4–15 kbar) and titanium contents (0.07–0.43 Ti p.f.u.). As in the case of the fbi end-member, regression analysis indicates that the P–T dependence of the Gibbs energy of tbi does not deviate significantly from that of the left-hand side of reaction (2), as adjusted for the configurational entropy of the reaction. The final regression analysis yields a Henry's law reference state Gibbs energy of formation from the elements (Eq. A.3, Appendix) for titanium–biotite of -5811.19 ± 2 kJ mol^{-1} at 298 K and 0.1 MPa.

Table 3. Representative microprobe analyses of minerals in samples VR 515, HO50 and H13.

Sample	Metapelitic hornfels		Quartz-free xenolith					High-pressure felsic granulite				
	VR 515		HO 50					H13				
	Grt	Bt	Grt core	Grt rim	Bt	Crd	Pl	Kfs	Pl	Bt	Grt core	Grt rim
wt%												
SiO_2	37.12	34.98	38.12	37.59	34.49	48.19	61.10	64.48	65.28	36.90	38.83	37.34
TiO_2	0.00	2.28	0.01	0.00	5.10	0.00	0.02	0.00	0.00	4.65	0.00	0.00
Cr_2O_3	0.00	0.00	0.04	0.00	0.04	0.02	0.07	0.00	0.00	0.00	0.00	0.00
Al_2O_3	20.94	19.26	21.22	21.38	18.64	32.29	24.82	18.24	21.95	18.39	21.80	21.75
FeO	32.20	21.07	36.60	36.25	23.01	11.74	0.04	0.04	0.00	15.48	25.83	28.30
MnO	6.62	0.13	0.74	0.90	0.04	0.10	0.00	0.00	0.00	0.00	0.58	0.98
MgO	2.13	8.21	3.59	3.34	6.14	6.64	0.02	0.00	0.00	11.57	7.12	5.45
CaO	2.02	0.00	1.13	1.14	0.02	0.01	6.55	0.03	3.16	0.00	5.95	5.39
Na_2O	0.00	0.26	0.03	0.07	0.29	0.11	7.15	1.31	9.86	0.00	0.00	0.00
K_2O	0.00	8.82	0.01	0.00	8.65	0.10	0.74	15.21	0.28	9.79	0.00	0.00
F	0.00	0.00	0.00	0.00	0.00	0.00	0.00	0.00	0.00	0.00	0.00	0.00
Cl	0.00	0.00	0.00	0.00	0.00	0.00	0.00	0.00	0.00	0.00	0.00	0.00
Total	101.03	95.02	101.50	100.67	96.42	99.20	100.51	99.31	100.52	96.78	100.11	99.21
Oxygen	12	8	12	12	11	18	8	8	8	11	12	12
Si	2.99	2.69	3.02	3.00	2.75	5.00	2.72	2.99	2.86	2.80	3.00	2.95
Ti	0.00	0.13	0.00	0.00	0.30	0.00	0.00	0.00	0.00	0.27	0.00	0.00
Cr	0.00	0	0.00	0.00	0.00	0.00	0.00	0.00	0.00	0.00	0.00	0.00
Al	1.97	1.75	1.98	2.01	1.75	3.95	1.30	1.00	1.13	1.64	1.98	2.03
Fe^{2+}	2.17	1.36	2.42	2.42	1.53	1.02	0.00	0.00	0.00	0.97	1.67	1.86
Mn	0.45	0.01	0.05	0.06	0.00	0.01	0.00	0.00	0.00	0.00	0.04	0.07
Mg	0.26	0.94	0.42	0.40	0.73	1.03	0.00	0.00	0.00	1.32	0.82	0.64
Ca	0.17	0.00	0.10	0.10	0.00	0.00	0.31	0.00	0.15	0.00	0.49	0.46
Na	0.00	0.04	0.00	0.01	0.04	0.02	0.62	0.12	0.84	0.00	0.00	0.00
K	0.00	0.87	0.00	0.00	0.89	0.01	0.04	0.90	0.02	0.95	0.00	0.00
F	0.00	0.00	0.00	0.00	0.00	0.00	0.00	0.00	0.00	0.00	0.00	0.00
Cl	0.00	0.00	0.00	0.00	0.00	0.00	0.00	0.00	0.00	0.00	0.00	0.00
Sum	8.00	7.77	8.00	8.00	8.00	11.04	5.00	5.00	5.00	7.95	8.00	8.00
X_{Fe}	0.89	0.59	0.85	0.86	0.68	0.50				0.42	0.67	0.74
X_{Grs}	0.06		0.03	0.03							0.16	0.12
X_{Alm}	0.71		0.79	0.81							0.55	0.61
X_{Prp}	0.08		0.14	0.13							0.27	0.22
X_{Sps}	0.15		0.02	0.02							0.01	0.02
X_{An}							0.32	0.00	0.15			
X_{Ab}							0.64	0.12	0.84			
X_{Or}							0.04	0.88	0.02			

© 2009 Blackwell Publishing Ltd

TEST OF THE BIOTITE MODEL

The quality of the reparameterized model is assessed in this section by comparing phase equilibria predicted by the model with natural and experimental observations. Because of the paucity of Mössbauer and wet chemical analyses for Fe^{3+} in the phases of interest, we focus almost exclusively on the Ti-content of biotite and $X_{Fe\ tot}(Fe/(Fe + Mg))$ values in co-existing Fe–Mg phases.

Test Samples

The experimental bulk compositions of Vielzeuf & Montel (1994) and Montel & Vielzeuf (1997) (Fig. 1a) are considered along with three natural amphibolite to granulite facies samples. Sample VR515 is a metapelitic hornfels from the southern contact aureole of the Vedrette di Ries Pluton in the Eastern Alps, Italy. Biotite in this rock is representative of a low metamorphic grade and is characterized by low Ti-content (0.13–0.14 p.f.u.). The mineralogy and metamorphic evolution of this amphibolite facies metapelite are summarized by Cesare (1994, 1999a,b). The observed assemblage Bt–Grt–And–Sil–St–Pl–Ms–Qtz–Ilm (mineral abbreviations after Kretz, 1983) includes metastable andalusite and staurolite, relicts from the prograde isobaric heating of the rock. The sample is from the incipient 'fibrolite–garnet zone' of Cesare (1999a), within which staurolite ultimately decomposes. These features are consistent with type 2bii in the facies series scheme proposed by Pattison & Tracy (1991), constraining the pressure of contact metamorphism in the range 3.5–4.5 kbar.

Sample HO50 is derived from El Hoyazo, SE Spain, where silica-undersaturated partially melted crustal xenoliths with well-preserved granulite facies Bt–Grt–Crd–Sil–Pl–Gr–Ilm quartz-free assemblage occur. The detailed geological framework, microstructures, evolution of mineral assemblages and *P–T* history of the investigated sample are described by Cesare *et al.* (1997, 2003, 2005, 2008). In this rock, cordierite appears to overgrow an earlier Bt–Grt–Sil–Pl–Ilm assemblage, most probably during a decompression event (Alvarez-Valero *et al.*, 2007). The *P–T* conditions for similar, Crd-free samples were estimated at 850 °C and 5–7 kbar on the basis of conventional thermobarometry (Cesare *et al.*, 1997) and independent experimental constraints (e.g. Ferri *et al.*, 2007). The HO50 sample offers a comprehensive database, obtained by Mössbauer spectroscopy, for the ferric iron contents of the co-existing phases (Cesare *et al.*, 2005), and therefore provides a simultaneous test of the capacity of the model to predict both Ti and ferric iron content.

Sample H13 is a felsic high-pressure Bt–Grt–Ky–Pl–Kfs–Qtz-bearing granulite from the Moldanubian zone in the Bohemian Massif (Czech Republic). This sample is a partly re-equilibrated silica-saturated, graphite-free rock that is described in detail by Tajčmanová *et al.* (2006, 2007, 2009), who estimated *P–T* conditions of 800–850 °C and 18 kbar from phase diagram sections computed for the Na_2O–CaO–K_2O–FeO–MgO–Al_2O_3–SiO_2–H_2O (NCKFMASH) system. This sample illuminates the topological consequences of the TiO_2 component for the phase diagram section.

Complete representative mineral compositions for all tested samples are shown in Table 3. The chemical parameters of relevance to the test of the model (atoms Ti, Fe^{3+}, X_{Fe}, X_{An}) are summarized in Table 4.

Methodology

P–T phase diagram sections were calculated for each test case. For the amphibolite facies metapelitic hornfels VR515, the model chemical system was MnO–Na_2O–CaO–K_2O–FeO–MgO–Al_2O_3–SiO_2–H_2O–TiO_2 (MnNCKFMASHT). Although the Mn-content of this rock is low, MnO was included in the modelling because of its influence on the stability of garnet (Spear, 1993; Tinkham *et al.*, 2001). For the granulite facies samples HO50 and H13, NCKFMASHTO and NCKFMASHT, respectively, were chosen as the chemical models. Manganese was neglected for these samples because it does not significantly influence phase relations at the conditions of interest. Fe^{3+} was considered only in the case of xenolith HO50, the only sample where a significant amount of Fe^{3+} in biotite (up to 10% of Fe^{3+}/Fe_{tot}; Cesare *et al.*, 2005) was measured by Mössbauer spectroscopy, and where Fe^{3+} data are available for the main Fe-bearing phases.

All calculations were done by Gibbs energy minimization (Connolly, 2005) with the thermodynamic database of Holland & Powell (1998, as revised 2003).

Table 4. Selected compositional parameters of key minerals in tested samples.

Sample	Metapelitic hornfels VR 515		Quartz-free xenolith HO50				High-pressure felsic granulite H13		
	Grt	Bt	$Grt_{(core-rim)}$	Bt	Crd	Pl	$Grt_{(core-rim)}$	Bt	Pl
Ti		0.13		0.27–0.3				0.26–0.28	
Fe^{3+}				0.07–0.21					
X_{Fe}	0.89	0.59–0.60	0.85–0.86	0.67–0.68	0.50		0.67–0.74	0.40–0.43	
X_{An}						0.31–0.32			0.15–0.17

© 2009 Blackwell Publishing Ltd

Unless noted otherwise, solution models are from White *et al.* (2000, 2002, 2007). For amphibolite facies sample VR515, the models of Newton *et al.* (1980) for plagioclase and Thompson & Hovis (1979) for K-feldspar were used, whereas calculations for HO50 and H13 were performed with the ternary feldspar model of Fuhrman & Lindsley (1988). For the hornfels VR515, Mn solution in chlorite, garnet and staurolite was accounted for by the Mn end-members introduced by Tinkham *et al.* (2001). The minor Mn solution observed in the natural biotite was neglected. An ideal model was used to account for the solution of Mn in ilmenite.

For the VR515 sample, the bulk composition was obtained by X-ray fluorescence, and for samples HO50 and H13, bulk compositions were estimated from analysed mineral compositions and their modal proportions derived from image analysis of backscattered electron (BSE) images. The resulting bulk-rock compositions (in mol.%) used for calculation are indicated in the upper left inset of calculated *P–T* phase diagram sections (Figs 3–5).

Phase equilibrium modelling

Experimental melting of metagreywacke

In the *P–T* phase diagram section (Fig. 1b) calculated with the revised biotite model for the bulk composition used in the experiments of Vielzeuf & Montel (1994), the biotite stability field extends to temperatures 30 to 50 °C higher than that predicted by the White *et al.* (2007) model (Fig. 1a), improving the match between experimental data and thermodynamic models. The calculated Ti-contents of biotite (Fig. 1b) are higher (up to Ti = 0.28 p.f.u.) than those calculated with the model of White *et al.* (2007; Fig. 1a) and are in better agreement with the experimentally observed compositions (see Table 2 in Montel & Vielzeuf, 1997 for details). Slight differences in the geometries of the *P–T* phase diagram sections of Fig. 1a,b are due to the use of different solution models for magnetite and feldspar.

Metapelitic hornfels (sample VR515)

The *P–T* section for VR515 (Fig. 3) was calculated assuming H_2O-saturated conditions. For this bulk composition, the increasing mode and Ti-content of biotite lead to the complete consumption of ilmenite at high temperatures. The stable mineral assemblage observed in the natural sample corresponds to the relatively large quadrivariant field Bt-Grt-Pl-Ms-Sil-

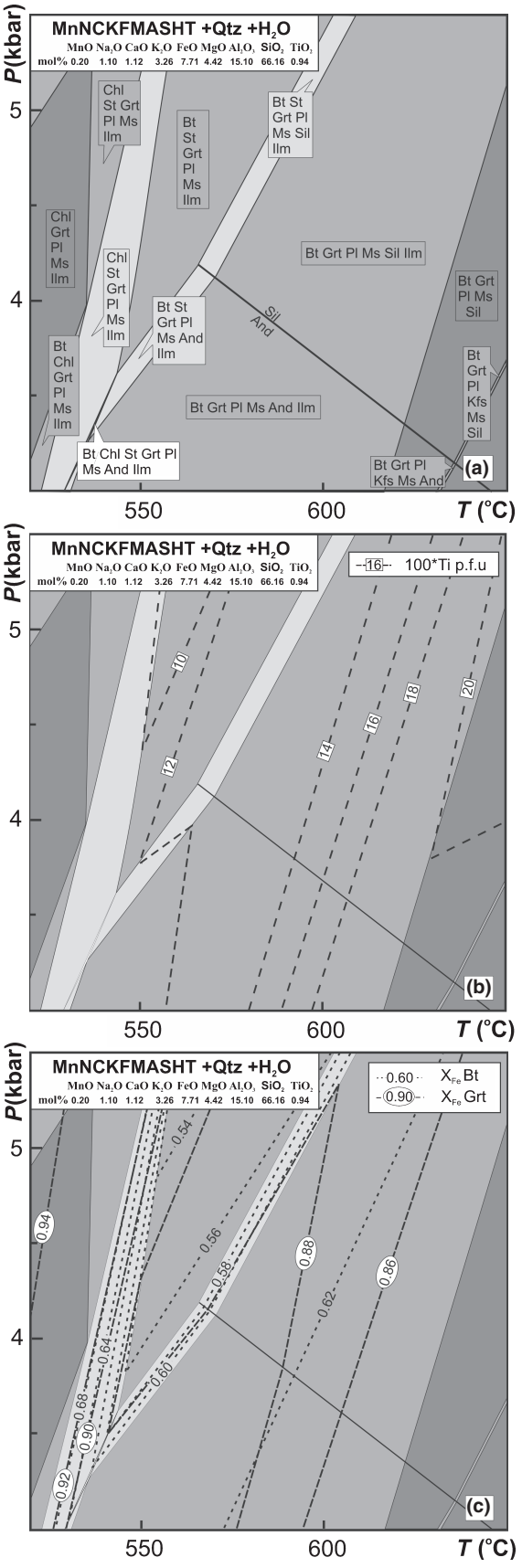

Fig. 3. (a) *P–T* section for metapelitic hornfels calculated for subsolidus mineral assemblage in MnNCKFMASHT system (with quartz and H_2O in excess). The observed mineral assemblage corresponds to the quadrivariant Bt-Grt-Pl-Ms-Sil-Ilm stability field. See text for details. (b) Contours for Ti p.f.u. of biotite. (c) Contours for X_{Fe} of biotite and garnet.

© 2009 Blackwell Publishing Ltd

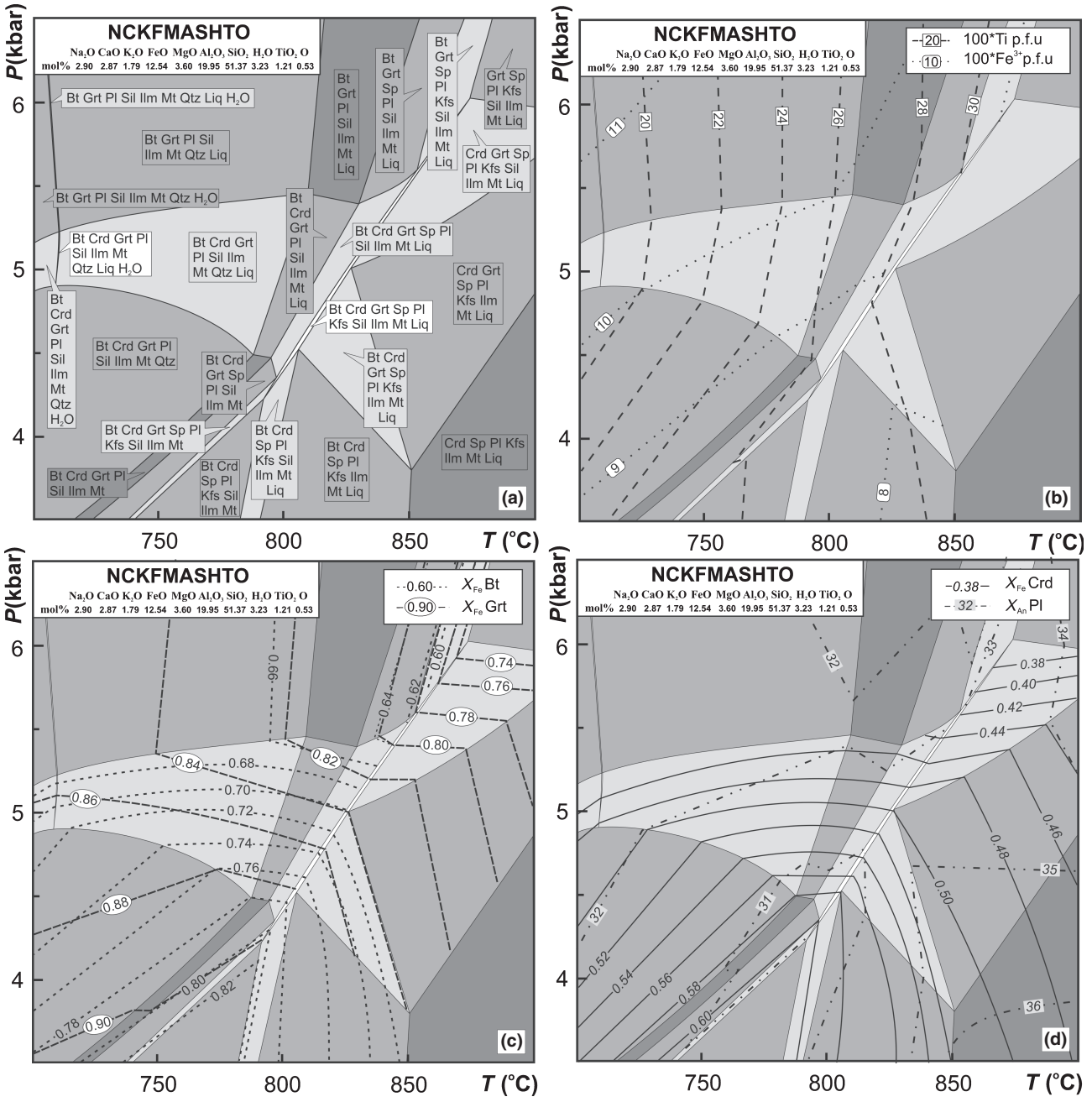

Fig. 4. (a) *P–T* section for silica-undersaturated xenoliths calculated in NCKFMASHTO system. The observed mineral assemblage corresponds to the quadrivariant Grt-Bt-Crd-Sil-Pl-Ilm-Mt-Liq stability field. See text for details. (b) Contours for Ti and Fe^{3+} p.f.u. of biotite. (c) Contours for X_{Fe} of biotite and garnet. (d) Contours for anorthite component in plagioclase and X_{Fe} of cordierite.

Ilm (+Qtz, H_2O). Given the composition of garnet (X_{Fe} = 0.88–0.89) and biotite (X_{Fe} = 0.59–0.60; Ti = 0.13–14 p.f.u.) the *P–T* conditions of equilibration of the observed mineral assemblage are 570–590 °C and 4.0–4.5 kbar. This *P–T* condition, based on intersection of isopleths, is consistent with the petrogenetic sequence of contact metamorphism inferred by Cesare (1999a), who proposed that the prograde sequence of AFM assemblages was Bt + St–Bt + St + And–Bt + St + Sil–Bt + Sil + Grt. This sequence is produced along an isobaric path at 4–4.2 kbar. The composition of biotite in this region of the Bt–Grt–Sil–Pl–Ms–Ilm (+Qtz, H_2O) stability field agrees with the composition of biotite in the natural sample (Fig. 3).

Quartz-free xenolith (sample HO50)

In the phase diagram section for the silica-undersaturated xenolith HO50 (Fig. 4), the observed

© 2009 Blackwell Publishing Ltd

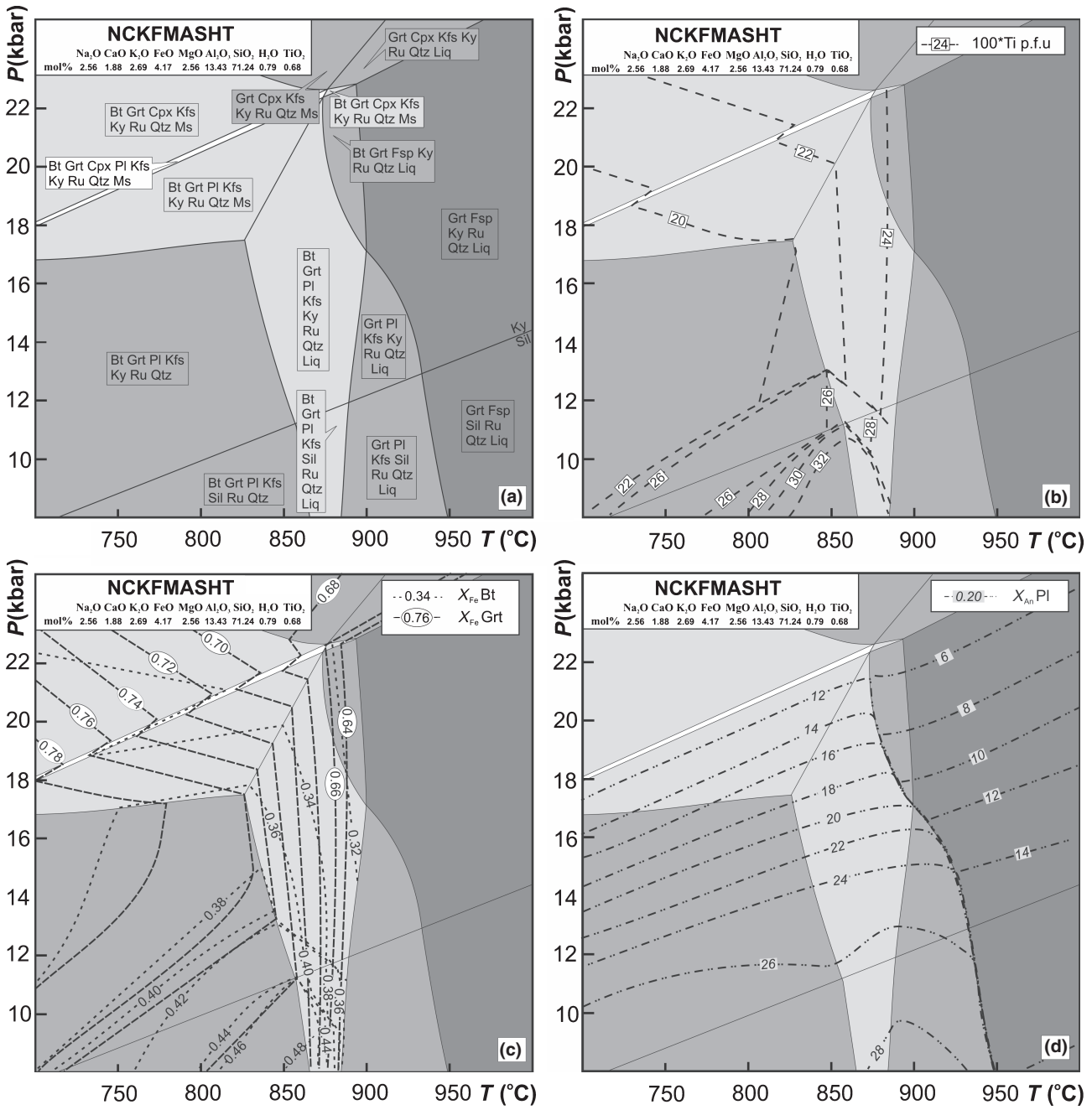

Fig. 5. (a) *P–T* section for felsic granulite from Bohemian Massif calculated in NCKFMASHT system. Fsp = potassium rich ternary feldspar. The observed mineral assemblage corresponds to the trivariant Grt-Bt-Ky-Kfs-Pl-Ru-Qtz-Liq stability field. See text for details. (b) Contours for Ti p.f.u. of biotite. (c) Contours for X_{Fe} of biotite and garnet. (d) Contours for anorthite component in plagioclase.

quartz-free mineral assemblage Grt–Bt–Crd–Sil–Pl–Ilm–Mt–Liq corresponds to a quadrivariant field in the middle of the diagram. Remarkably, the relevant compositional isopleths of garnet (X_{Fe} = 0.85–0.86), biotite (X_{Fe} = 0.67–0.68; Ti = 0.27–0.30 p.f.u.; Fe^{3+} = 0.07–0.21 p.f.u.), cordierite (X_{Fe} = 0.50) and plagioclase (An = 31–32 mol.%) cross consistently in this quadrivariant field, indicating that sample HO50 equilibrated at 790–825 °C and 5 kbar.

High-pressure felsic granulite (sample H13)

The *P–T* section for H13 felsic granulite (Fig. 5) is calculated for the bulk composition of Tajčmanová *et al.* (2006) and is characterized by a simple mineralogy as originally modelled by Tajčmanová *et al.* (2006, their fig. 7). The trivariant Grt–Bt–Ky–Kfs–Pl–Ru–Qtz–Liq field corresponds to the observed high-pressure mineral assemblage in the rock, where

© 2009 Blackwell Publishing Ltd

the isopleths of measured X_{Fe} in the cores of garnet relics (X_{Fe} = 0.64–0.68) and anorthite component in plagioclase (An = 15–16 mol%) indicate conditions of 850–880 °C and 18 kbar. However, the observed biotite compositions (X_{Fe} = 0.40–0.43; Ti = 0.26–0.28 p.f.u.) are indicative of somewhat lower pressures (around 12 kbar) within the same trivariant field, a discrepancy attributed to the re-equilibration during exhumation as suggested by Tajčmanová *et al.* (2006). The main difference between the current phase relations (Fig. 5) and those of Tajčmanová *et al.* (2006; their fig. 7) is that, as a consequence of the expansion of the biotite stability field, biotite is predicted to be a stable constituent of the peak pressure assemblage. Nonetheless, the *P–T* evolution estimated using the peak garnet-plagioclase and re-equilibrated biotite compositions remains unchanged (see Tajčmanová *et al.*, 2006, for details).

SUMMARY AND DISCUSSION

The biotite thermodynamic model of White *et al.* (2007) was modified to account for ordering of Ti onto the M2 octahedral site rather than the M1 site as previously assumed. Making use of the KFMASH biotite model of Holland & Powell (2006) as a basis, after adjusting the estimate for the enthalpy of the ordering reaction, the modified model was reparameterized for titanium and ferric iron solution. Specifically, the Gibbs energy of the Ti-biotite end-member was estimated from biotite with a wide range of Ti-contents (Williams & Grambling, 1990; Vielzeuf & Montel, 1994; Patiño Douce & Beard, 1995). The calibration of the Fe^{3+} end-member was complicated by the paucity of suitable data and based entirely on observations from natural biotite (Williams & Grambling, 1990). In both cases, Henry's law reference state Gibbs energies of formation were derived.

The resulting model has been tested against a wide range of natural samples. The samples were chosen to characterize different metamorphic grades and bulk compositions. The results of these tests (Figs 3–5) demonstrate that the model realistically portrays biotite compositions in the majority of samples. When compared with results obtained with the original model (Fig. 1a), isopleths of Ti- and Fe^{3+}-content in biotite computed with the new model in biotite are in significantly better agreement with observed compositions from the experiments of Vielzeuf & Montel (1994; Fig. 1b).

The new model performs less well for extreme Ti-contents. For biotite with high Ti-content (> 0.35 p.f.u.), the resulting isopleths are underestimated by up to 0.05 Ti p.f.u. The calibration of the Fe^{3+} end-member should be regarded with caution because of the limited amount of data available on the Fe^{3+}-content of relevant phases. In particular, it is to be expected that the model's predictive power will be limited when applied to samples with high ferric iron contents. Future advances in understanding the exchanges and site distributions of Fe^{3+} and Al as well as dioctahedral and talc substitution, that become important at high pressure (Hermann, 2002; Comodi *et al.*, 2004), will permit further improvement of the biotite solution model.

ACKNOWLEDGEMENTS

We thank D. Tinkham and D. Vielzeuf for constructive reviews and G. Cruciani and B. Ciervo for extensive discussion on biotite crystal chemistry. Financial support for this project was provided by the University of Padova (Assegni di Ricerca 2006-CPDR069917), Italian MIUR (PRIN2007-2007278A22), Consiglio Nazionale delle Ricerche, and Swiss National Science Funds grant 200021-107889.

REFERENCES

Alvarez-Valero, A. M., Cesare, B. & Kriegsman, L. M., 2007. Formation of spinel-cordierite-feldspar-glass coronas after garnet in metapelitic xenoliths: reaction modelling and geodynamic implications. *Journal of Metamorphic Geology*, **25,** 305–320.

Berman, R. G., Aranovich, L. Y., Rancourt, D. G. & Mercier, P. H. J., 2007. Reversed phase equilibrium constraints on the stability of Mg-Fe-Al biotite. *American Mineralogist*, **92,** 139–150.

Brigatti, M. F. & Guggenheim, S., 2002. Mica crystal chemistry and the influence of pressure, temperature, and solid solution on atomistic models. In: *Micas: Crystal Chemistry and Metamorphic Petrology*. *Reviews in Mineralogy and Geochemistry 45* (eds Mottana, A., Sassi, F., Thompson, J. & Guggenheim, S.), pp. 1–97. Mineralogical Society of America, Washington, DC.

Brigatti, M. F., Lugli, C., Poppi, L., Foord, E. E. & Kile, D. E., 2000a. Crystal chemical variations in Li- and Fe-rich micas from Pikes Peak batholith (central Colorado). *American Mineralogist*, **85,** 1275–1286.

Brigatti, M. F., Frigieri, P., Ghezzo, C. & Poppi, L., 2000b. Crystal chemistry of Al-rich biotites coexisting with muscovites in peraluminous granites. *American Mineralogist*, **85,** 436–448.

Carswell, D. A. & O'Brien, P. J., 1993. Thermobarometry and geotectonic significance of high-pressure granulites – example from the Moldanubian zone of the Bohemian massif in Lower Austria. *Journal of Petrology*, **34,** 427–459.

Cesare, B., 1994. Hercynite as the product of staurolite decomposition in the contact aureole of Vedrette di Ries, eastern Alps, Italy. *Contributions to Mineralogy and Petrology*, **116,** 239–246.

Cesare, B., 1999a. Multi-stage pseudomorphic replacement of garnet during polymetamorphism: 1. Microstructures and their interpretation. *Journal of Metamorphic Geology*, **17,** 723–734.

Cesare, B., 1999b. Multi-stage pseudomorphic replacement of garnet during polymetamorphism: 2. Algebraic analysis of mineral assemblages. *Journal of Metamorphic Geology*, **17,** 735–746.

Cesare, B., Salvioli-Mariani, E. & Venturelli, G., 1997. Crustal anatexis and melt segregation in the restitic xenoliths at El Hoyazo (SE Spain). *Mineralogical Magazine*, **61,** 15–27.

Cesare, B., Cruciani, G. & Russo, U., 2003. Hydrogen deficiency in Ti-rich biotite from anatectic metapelites

© 2009 Blackwell Publishing Ltd

(El Joyazo – SE Spain): crystal-chemical aspects and implications for high-temperature petrogenesis. *American Mineralogist*, **88,** 583–595.

Cesare, B., Meli, S., Nodari, L. & Russo, U., 2005. Fe^{36+} reduction during biotite melting in graphitic metapelites: another origin of CO_2 in granulites. *Contributions to Mineralogy and Petrology*, **149,** 129–140.

Cesare, B., Satish-Kumar, M., Cruciani, G., Shabeer, P. & Nodari, L., 2008. Mineral chemistry of Ti-rich biotite from pegmatite and metapelitic granulites of the Kerala Khondalite Belt (SE India): petrology and further insight into titanium substitutions. *American Mineralogist*, **93,** 327–338.

Circone, S. & Navrotsky, A., 1992. Substitution of $^{[6,4]}$ Al in phlogopite: high temperature solution calorimetry, heat capacities, and thermodynamic properties of the phlogopite-eastonite join. *American Mineralogist*, **77,** 1191–1205.

Clarke, G. L., Powell, R. & Guiraud, M., 1989. Low-pressure granulite facies metapelitic assemblages and corona textures from MacRobertson Land, east Antarctica: the importance of Fe_2O_3 and TiO_2 in accounting for spinel-bearing assemblages. *Journal of Metamorphic Geology*, **7,** 323–335.

Coggon, R. & Holland, T. J. B., 2002. Mixing properties of phengitic micas and revised garnet–phengite thermobarometers. *Journal of Metamorphic Geology*, **20,** 683–696.

Comodi, P., Fumagalli, P., Montagnoli, M. & Zanazzi, P. F., 2004. A single-crystal study on the pressure behavior of phlogopite and petrological implications. *American Mineralogist*, **89,** 647–653.

Connolly, J. A. D., 2005. Computation of phase equilibria by linear programming: a tool for geodynamic modeling and its application to subduction zone decarbonation. *Earth and Planetary Science Letters*, **236,** 524–541.

Cruciani, G. & Zanazzi, P. F., 1994. Cation partitioning and substitution mechanisms in 1 M phlogopite; a crystal chemical study. *American Mineralogist*, **79,** 289–301.

Ferri, F., Burlini, L., Cesare, B. & Sassi, R., 2007. Seismic properties of lower crustal xenoliths from El Hoyazo (SE Spain): experimental evidence up to partial melting. *Earth and Planetary Science Letters*, **253,** 239–253.

Fuhrman, M. L. & Lindsley, D. H., 1988. Ternary-feldspar modeling and thermometry. *American Mineralogist*, **73,** 201–215.

Guidotti, C. V. & Dyar, M. D., 1991. Ferric iron in metamorphic biotite and its petrologic and crystallochemical implications. *American Mineralogist*, **76,** 161–175.

Harley, S. L., 1989. The origins of granulites: a metamorphic perspective. *Geological Magazine*, **126,** 215–331.

Hermann, J., 2002. Experimental constraints on phase relations in subducted continental crust. *Contributions to Mineralogy and Petrology*, **143,** 219–235.

Holland, T. J. B. & Powell, R., 1998. An internally consistent thermodynamic data set for phases of petrological interest. *Journal of Metamorphic Geology*, **16,** 309–343.

Holland, T. J. B. & Powell, R., 2003. Activity-composition relations for phases in petrological calculations: an asymmetric multicomponent formulation. *Contributions to Mineralogy and Petrology*, **145,** 492–501.

Holland, T. J. B. & Powell, R., 2006. Petrological calculations involving Fe-Mg equipartition in multisite minerals: a logical inconsistency. *Journal of Metamorphic Geology*, **24,** 851–861.

Kretz, R., 1983. Symbols for rock forming minerals. *American Mineralogist*, **68,** 277–279.

Lasaga, A. C. & Burnham, C. W., 1979. Water and magmas – clarification of a controversy of applications of the Gibbs-Duhem equation – reply. *Geochimica et Cosmochimica Acta*, **43,** 643–647.

Laurora, A., Brigatti, M. F., Mottana, A., Malferrari, D. & Caprilli, E., 2007. Crystal chemistry of trioctahedral micas in alkaline and subalkaline volcanic rocks: A case study from Mt. Sassetto (Tolfa district, Latium, central Italy). *American Mineralogist*, **92,** 468–480.

Mercier, P. H. J., Rancourt, D. G., Redhammer, G. J. *et al.*, 2006. Upper limit of the tetrahedral rotation angle and factors affecting octahedral flattening in synthetic and natural 1M polytype C2/m space group micas. *American Mineralogist*, **91,** 831–849.

Mesto, E., Schingaro, E., Scordari, F. & Ottolini, L., 2006. An electron microprobe analysis, secondary ion mass spectrometry, and single-crystal X-ray diffraction study of phlogopites from Mt. Vulture, Potenza, Italy: Consideration of cation partitioning. *American Mineralogist*, **91,** 182–190.

Montel, J. M. & Vielzeuf, D., 1997. Partial melting of metagreywackes. II. Compositions of minerals and melts. *Contributions to Mineralogy and Petrology*, **128,** 176–196.

Newton, R. C., Charlu, T. V. & Kleppa, O. J., 1980. Thermochemistry of high structural state plagioclases. *Geochimica et Cosmochimica Acta*, **44,** 933–941.

Patiño Douce, A. E. & Beard, J. S., 1995. Dehydration-melting of biotite gneiss and quartz amphibolite from 3 to 15 kbar. *Journal of Petrology*, **36,** 707–738.

Patiño Douce, A. E. & Beard, J. S., 1996. Effects of P, $f(O_2)$ and Mg/Fe ratio on dehydration melting of model metagreywackes. *Journal of Petrology*, **37,** 999–1024.

Patiño Douce, A. E. & Johnston, A. D., 1991. Phase equilibria and melt productivity in the pelitic system: implications for the origin of peraluminous granitoids. *Contributions to Mineralogy and Petrology*, **107,** 202–218.

Patiño Douce, A. E., Johnston, A. & Rice, J. M., 1993. Octahedral excess mixing properties in biotite; a working model with applications to geobarometry and geothermometry. *American Mineralogist*, **78,** 113–131.

Pattison, D. R. M. & Tracy, R. J., 1991. Phase equilibria and thermobarometry of metapelites. In: *Contact Metamorphism, Reviews in Mineralogy 26*, (ed. Kerrick, D. M.), pp. 105–206. Mineralogical Society of America, Washington, DC.

Pitra, P. & de Waal, S. A., 2001. High-temperature, low-pressure metamorphism and development of prograde symplectites, Marble Hall Fragment, Bushveld Complex (South Africa). *Journal of Metamorphic Geology*, **19,** 311–325.

Powell, R. & Holland, T. J. B., 1999. Relating formulations of the thermodynamics of mineral solid solutions; activity modeling of pyroxenes, amphiboles and micas. *American Mineralogist*, **84,** 1–14.

Powell, R. & Holland, T. J. B., 2004. *Course Notes for "THERMOCALC Workshop 2004: Calculating Metamorphic Phase Equilibria"* (CD ROM). ETH, Zurich.

Powell, R., Holland, T. J. B. & Worley, B., 1998. Calculating phase diagrams involving solid solutions via non- linear equations, with examples using THERMOCALC. *Journal of Metamorphic Geology*, **16,** 577–588.

Scordari, F., Ventruti, G., Sabato, A., Bellatreccia, F., Della Ventura, G. & Pedrazzi, G., 2006. Ti-rich phlogopite from Monte Vulture (Potenza, Italy) investigated by a multianalytical approach: substitutional mechanisms and orientation of the OH dipoles. *European Journal of Mineralogy*, **18,** 379–391.

Spear, F. S., 1993. *Metamorphic Phase Equilibria and Pressure–Temperature–Time Paths*. Mineralogical Society of America, Washington, DC, pp. 353–354.

Stevens, G., Clemens, J. C. & Droop, G. T. R., 1997. Melt production during granulite-facies anatexis: experimental data from "primitive" metasedimentary protoliths. *Contributions to Mineralogy and Petrology*, **128,** 352–370.

Tajčmanová, L., Konopásek, J. & Schulmann, K., 2006. Thermal evolution of the orogenic lower crust during exhumation within a thickened Moldanubian root of the Variscan belt of Central Europe. *Journal of Metamorphic Geology*, **24,** 119–134.

Tajčmanová, L., Konopásek, J. & Connolly, J. A. D., 2007. Diffusion-controlled development of silica-undersaturated domains in felsic granulites of the Bohemian Massif (Variscan belt of Central Europe). *Contributions to Mineralogy and Petrology*, **153,** 237–250.

Tajčmanová, L., Konopásek, J. & Košler, J., 2009. Mobility of zinc and its role in stabilization of spinel-bearing mineral

© 2009 Blackwell Publishing Ltd

assemblages in high-grade felsic rocks of the Moldanubian domain (Bohemian Massif). *European Journal of Mineralogy*, doi: 10.1127/0935-1221/2009/0021-1899.
Thompson, J. B. & Hovis, G. L., 1979. Entropy of Mixing in Sanidine. *American Mineralogist*, **64,** 57–65.
Tinkham, D. K., Zuluaga, C. A. & Stowell, H. H., 2001. Metapelite phase equilibria modeling in MnNCKFMASH: The effect of variable Al_2O_3 and MgO/(MgO + FeO) on mineral stability. *Geological Materials Research*, **3,** 1–42.
Toraya, H., 1981. Distortions of octahedra and octahedral sheets in 1M micas and the relation to their stability. *Zeitschrift für Kristallographie*, **157,** 173–190.
Ventruti, G., Levy, D., Pavese, A., Scordari, F. & Suard, E., 2009. High-temperature treatment, hydrogen behaviour and cation partitioning of a Fe-Ti bearing volcanic phlogopite by in situ neutron powder diffraction and FTIR spectroscopy. *European Journal of Mineralogy*.doi: 10.1127/0935-1221/2009/0021-1903.
Vielzeuf, D. & Clemens, J. D., 1992. The fluid-absent melting of phlogopite + quartz: experiments and models. *American Mineralogist*, **77,** 1206–1222.
Vielzeuf, D. & Montel, J. M., 1994. Partial melting of metagreywackes. I. Fluid-absent experiments and phase relationships. *Contributions to Mineralogy and Petrology*, **117,** 375–393.
Virgo, D. & Popp, R. K., 2000. Hydrogen deficiency in mantle-derived phlogopites. *American Mineralogist*, **85,** 753–759.
Waters, D. J. & Charnley, N. R., 2002. Local equilibrium in polymetamorphic gneiss and the titanium substitution in biotite. *American Mineralogist*, **87,** 383–396.
White, R. W., Powell, R., Holland, T. J. B. & Worley, B. A., 2000. The effect of TiO_2 and Fe_2O_3 on metapelitic assemblages at greenschist and amphibolite facies conditions: mineral equilibria calculations in the system K_2O-FeO-MgO-Al_2O_3-SiO_2-H_2O-TiO_2-Fe_2O_3. *Journal of Metamorphic Geology*, **18,** 497–511.
White, R. W., Powell, R. & Clarke, G. L., 2002. The interpretation of reaction textures in Fe-rich metapelitic granulites of the Musgrave Block, central Australia: constraints from mineral equilibria calculations in the system K_2O-FeO-MgO-Al_2O_3-SiO_2-H_2O-TiO_2-Fe_2O_3. *Journal of Metamorphic Geology*, **20,** 41–55.
White, R. W., Powell, R. & Holland, T. J. B., 2007. Progress relating to calculation of partial melting equilibria for metapelites. *Journal of Metamorphic Geology*, **25,** 511–527.
Williams, M. L. & Grambling, J. A., 1990. Manganese, ferric iron, and the equilibrium between garnet and biotite. *American Mineralogist*, **75,** 886–908.

APPENDIX

The KFMASHTO biotite solution model

The molar Gibbs energy of the biotite solution model may be expressed as

$$G^{\text{bio}} = G^{\text{mech}} + G^{\text{conf}} + G^{\text{excess}} \qquad (A.1)$$

where G^{mech} is the energy arising from mechanical mixing of the end-members; G^{conf} is the energy expected to arise from theoretical entropic considerations; and G^{excess} is an empirical term accounting for strain energy and deviations from the theoretical model. The mechanical mixing term is

$$G^{\text{mech}} = \sum_i p_i G_i^{\circ} \qquad (A.2)$$

where p_i and G_i° are the molar proportion and Gibbs energy of the pure end-members ann, phl, east, obi, tbi and fbi (Table 1). The Gibbs energies of ann, phl and east are taken directly from Holland & Powell (1998, as revised 2003), and the Gibbs energies of obi, tbi and fbi are computed as

$$G_i^{\circ} = G_{\text{lhs}_i}^{\circ} + \delta H_i - T\delta S_i \qquad (A.3)$$

where $G_{\text{lhs}_i}^{\circ}$ is the Gibbs energy of the linear combination of end-members on the left-hand side of reactions (1), (2) and (3) for obi, fbi and tbi, respectively, as computed from the data of Holland & Powell (1998, as revised 2003) at the pressure and temperature of interest. δS_{obi} and δS_{fbi} are zero, the remaining values of δH_i and δS_i were constrained as discussed in the text and are summarized in Table A1. In the case of the obi end-member, δH_{obi} is identical to the enthalpy of ordering, $\Delta H^0_{\text{order}}$, for reaction (1). The configurational term of eq. (A.1) is

Table A1. Biotite solution model parameters.

$W_{\text{phl-ann}}$	12 kJ mol^{-1}
$W_{\text{phl-east}}$	10 kJ mol^{-1}
$W_{\text{phl-obi}}$	4 kJ mol^{-1}
$W_{\text{ann-east}}$	3 kJ mol^{-1}
$W_{\text{ann-obi}}$	8 kJ mol^{-1}
$W_{\text{obi-east}}$	7 kJ mol^{-1}
δH_{obi}	−6.8 kJ mol^{-1}
δS_{obi}	0
δH_{tbi}	84 kJ mol^{-1}
δS_{tbi}	11.5 J K^{-1} mol^{-1}
δH_{fbi}	6 kJ mol^{-1}
δS_{fbi}	0

$$G^{\text{conf}} = -T\left(S^{\text{conf}} - S^{\text{mech}}\right) \qquad (A.4)$$

where S^{conf} and S^{mech} are the configurational entropy of the solution and a mechanical mixture of the end-members, respectively. The configurational entropy of the solution is

$$S^{\text{conf}} = -R\sum_i \sum_{j=1}^{m_i} q_i z_{ij} \ln z_{ij} \qquad (A.5)$$

where i indexes the crystallographic sites in biotite on which independent mixing is assumed to occur (M1, M2, T1, H; Table 1); q_i is the multiplicity of each site; m_i is the number of species that mix on each site; and z_{ij} is the atomic fraction of the jth species on the ith site. The site multiplicities and species on each site are indicated in Table 1 and the site fractions z_{ij} can be expressed as a function of the end-member proportions from the knowledge of the site populations of the pure end-members. The configuration of a mechanical mixture of the end-members is

$$S^{\text{mech}} = \sum_i p_i S_i^{\text{conf}} \qquad (A.6)$$

where S_i^{conf} is the configurational entropy of the end-member as deduced from the site

© 2009 Blackwell Publishing Ltd

occupancies indicated in Table 1. The excess term of eq. (A.1) is

$$G^{\text{excess}} = \sum_{i} \sum_{j=1}^{i-1} W_{ij} p_i p_j \qquad \text{(A.7)}$$

where the non-zero interaction terms W_{ij} (Table A1) are taken from the parameterization of Holland & Powell (2006).

Because the end-members of the biotite solution model are compositionally degenerate, the proportions of the end-members must be determined by finding the proportions that minimize the total energy of the solution. This may be accomplished by expressing the bulk composition in terms of the proportions of the end-members for the fully disordered state ($Q = 0$). Designating these proportions as p_i^0, and making use of the stoichiometric constraint imposed by reaction (1), the stable speciation

$$\begin{aligned} p_{\text{phl}} &= p^0_{\text{phl}} - 2\delta p_{\text{obi}}/3 \\ p_{\text{ann}} &= p^0_{\text{ann}} - \delta p_{\text{obi}}/3 \\ p_{\text{obi}} &= p^0_{\text{obi}} + \delta p_{\text{obi}} \\ p_{\text{east}} &= p^0_{\text{east}},\ \ p_{\text{tbi}} = p^0_{\text{tbi}},\ \ p_{\text{fbi}} = p^0_{\text{fbi}} \end{aligned} \qquad \text{(A.8)}$$

is a function of the fully disorder speciation and is unknown. The unknown quantity δp_{obi} is determined by solving

$$\frac{\partial G^{\text{bio}}}{\partial \delta p_{\text{obi}}} = 0 \qquad \text{(A.9)}$$

by making use of eqs (A.1–A.8) to express G^{bio} as a function of δp_{obi}.

Received 1 October 2008; revision accepted 24 December 2008.

© 2009 Blackwell Publishing Ltd